

Wireless Side-Lobe Eavesdropping Attacks

Yanzi Zhu, Ying Ju^{§†}, Bolun Wang, Jenna Cryan[‡], Ben Y. Zhao[‡], Haitao Zheng[‡]
 University of California, Santa Barbara [§]Xi'an Jiaotong University
[†]State Radio Monitoring Center [‡]University of Chicago
 {yanzi, bolunwang}@cs.ucsb.edu, juyingtju@163.com,
 {jennacryan, ravenben, htzheng}@cs.uchicago.edu

ABSTRACT

Millimeter-wave wireless networks offer high throughput and can (ideally) prevent eavesdropping attacks using narrow, directional beams. Unfortunately, imperfections in physical hardware mean today's antenna arrays all exhibit side lobes, signals that carry the same sensitive data as the main lobe. Our work presents results of the first experimental study of the security properties of mmWave transmissions against side-lobe eavesdropping attacks. We show that these attacks on mmWave links are highly effective in both indoor and outdoor settings, and they cannot be eliminated by improved hardware or currently proposed defenses.

1. INTRODUCTION

Wireless communication has always been more vulnerable to attacks than its wired counterparts. The fact that wireless signals are broadcast means they are more easily eavesdropped. This weakness has been exploited in many wireless networks [33, 34, 36]. Even more recent security protocols like WPA2-PSK have been successfully compromised by snooping attacks [11, 30] via simple tools [2]. Despite existing encryptions, one can still infer the specific sources of traffic by observing just packet sizes and counts in data transmissions [17, 28].

While we continue to improve encryption algorithms, an equally promising direction is to use wireless beamforming to defend against eavesdroppers at the physical layer. Beamforming allows a transmitter (TX) to send a highly focused, directional signal towards a target receiver (RX), so that nearby attackers not directly between the two endpoints cannot capture the transmission. The narrow beam is built by leveraging signal cancellations among multiple antennas in a phased array¹, and is most easily built on *millimeter-wave* (mmWave) transmitters [1]. For example, 60GHz phased arrays could fit on small devices like smartphones, and can generate highly focused beams (*e.g.*, 3° using 32×32 antennas) while achieving Gbps throughput.

While earlier applications focused on short-range indoor applications, *e.g.*, home routers [8] and wireless virtual reality headsets [10], new applications of mmWave leverage its high directionality and throughput for long-range communi-

¹ We do not consider horn antennas as they are bulky, expensive, and can only be rotated mechanically. They are not suitable for our application scenarios.

cation. Many such applications have already been deployed. Facebook has deployed a mesh network using 60GHz communications in downtown San Jose [7]. Google is considering replacing wired fiber with mmWave to reduce cost [5]. Academics have proposed picocell networks using mmWave signals towards next 5G network [29, 32, 42].

With a growing number of deployed networks and applications, understanding physical properties of mmWave is critical. One under-studied aspect of directional transmissions is the artifact of array *side lobes*. Fig. 1 shows an example of the series of side lobes pointing in different directions. Side lobes are results of imperfect signal cancellation among antenna elements. While weaker than the main lobe, side lobes carry the same information, and can be exploited by eavesdroppers to recover the transmission. As physical imperfections, they are very difficult to eliminate.

In this paper, we conduct the first empirical study of the security properties of mmWave communications against side-lobe eavesdropping attacks. While theoretical studies have shown the problem of side-lobe leakage [25], it is never validated using network measurements, especially for long-range communications. We use a commercial 60GHz testbed from Facebook's Terragraph project [4] to evaluate the effectiveness of side-lobe eavesdropping in both indoor and outdoor scenarios. Specifically, we answer three key questions:

- **How severe is mmWave side-lobe eavesdropping? (§3)**

We observe that side-lobe eavesdropping is incredibly effective in both indoor and outdoor scenarios. Attacker can recover transmission in a large area with high success rate (details below). Particularly for outdoor scenarios, most eavesdropping areas are connected, and the attacker can move freely and launch stealthy attacks.

Eavesdropping Area (m^2)	Attacker's Packet Success Rate		
	>10%	>50%	>95%
Mesh	79	64.6	55
Picocell	109	88.6	54
Peer-to-Peer	16.6	15.7	13.1

- **Can better mmWave hardware improve security? (§4)**

We find that improved hardware can only reduce the impact of the eavesdropping attack, but not fully defend against it. Eavesdropping side lobes is still possible even after removing hardware artifacts from antennas and deploying more antenna elements.

- **Are existing defenses effective against side-lobe eavesdropping attacks? (§5)** Although existing defenses show

promising results against single-device eavesdroppers, they either impose impractical hardware requirements, or remain vulnerable against more advanced attackers, *e.g.*, those with multiple devices.

2. BACKGROUND

To provide context for later study, we first describe the adversarial model and then our measurement methodology.

Adversarial Model. We consider *passive* eavesdropping, where an attacker listens to side-lobe signals and recovers packet header or payload. The attacker stays hidden from its victim TX and RX, but is unable to manipulate the communication between the victims. Without knowing the attacker’s physical location, victims cannot apply conventional defenses like null-forming².

We do not consider eavesdropping attacks on the main lobe of the transmission. Such an attack would affect the communication between TX and RX, as the attacker has to stay inside the main lobe or use a reflector, and thus can be detected [35]. Finally, we assume the attacker has one or more synchronized devices as powerful as the victim’s hardware. The attacker knows the victim’s location and hardware configuration³. The attacker and his device(s) are free to move around the victims.

Application Scenarios. We consider three practical scenarios where mmWave signals are commonly used: mesh networks [7], picocell networks [42], and indoor peer-to-peer transmissions [8, 10]. Fig. 2 shows an illustration of the three.

mmWave signals are commonly considered for indoor peer-to-peer scenarios (Fig. 2(c)), *e.g.*, virtual reality [10, 12] and wireless display [3]. Here TX and RX are within very short range ($\leq 10\text{m}$) and often at the same height ($\sim 1\text{m}$). As mmWave signals degrade much faster than lower frequency signals in the air, it is less known that they can also be used outdoor for long-range communications (20–200m). For example, Facebook has deployed a mesh network in downtown San Jose [7], supporting up to 200m link using 60GHz phased array radios⁴. Researchers [29, 42] also propose picocell networks using 60GHz signals. In both scenarios, TX is mounted higher than human height, *e.g.*, 6m. Depending on the scenario, RX is either mounted at a similar height or on the ground, shown in Fig. 2(a) and (b), respectively.

Measurement Hardware. Our testbed consists of three identical 60GHz radios. We use them as TX, RX, and the attacker. Each radio has a 16×8 rectangular phased array (Fig. 3) and follows the 802.11ad single-carrier standard for 60GHz communication [6]. Our radios are designed for outdoor mesh network scenario with a maximum Equivalent

²If TX knows the attacker’s location, it can change its radiation pattern to nullify signals towards that location to avoid attacks [15].

³This information is often publicly available, or could be derived from simple techniques, *e.g.*, device localization.

⁴Compared to horn antennas, phased arrays offer robust real-time link adaptation by eliminating mechanical steering.

Scenario	TX		RX			Examined Area (m ²)
	EIRP (dBm)	Height (m)	Distance to TX (m)	Height (m)	Max Throughput (Gbps)	
Mesh	32	6	200	6	1.0	10×20
Picocell	32	6	50	1	1.5	10×20
Peer-to-Peer	23	1	10	1	1.5	4×5

Table 1: Detailed experiment setup and configurations.

Isotropically Radiated Power (EIRP) of 32dBm, supporting 1Gbps (QPSK) transmissions at 200m range (line-of-sight). But we could re-purpose these radios for picocell and peer-to-peer scenarios as well, by lowering the EIRP. Each receiving radio can report received signal-to-noise-ratio (SNR) of each packet in real time.

Measurement Setup. We place our testbed radios at different heights and distances apart to emulate the three application scenarios. In all scenarios, TX sends 32KB TCP packets to RX at 1Gbps by default. Equipment placement details and specifications are listed in Table 1. In particular for (c) peer-to-peer, we choose 23dBm EIRP the same as the commodity 60GHz chipset from Wilocity [9]. Given TX’s EIRP and the distance from victim RX to TX, RX can at best communicate with TX at 1Gbps, 1.5Gbps, and 1.5Gbps with less than 5% packet loss in mesh, picocell, and peer-to-peer networks, respectively. Further reducing TX power will affect RX’s performance.

During transmission, we move the attacker radio around TX to eavesdrop side lobes at different locations. We grid the area around TX (200m^2 for two outdoor scenarios and 20m^2 for the indoor scenario) into 816 (34×24) rectangles. In each grid, we face the attacker radio at TX and eavesdrop the transmission for 30s. Our testbed could record 100k packet samples and 30 SNR values in each grid. In each application scenario, we collected a total of 80 million packets and 24k SNR measurements.

3. EFFECTIVENESS OF EAVESDROPPING

From our collected measurements, we now present the severity of side-lobe eavesdropping under three mmWave network scenarios. We use the following two metrics to quantify the effectiveness of side-lobe eavesdropping.

- *Packet success rate (PSR)* measures the percentage of packets the attacker could successfully retrieve from eavesdropping through side lobes, calculated from 100k packets per location. When the attacker’s PSR is no less than that of the victim RX ($>95\%$ in our experiments), we consider it to be a *full* attack.
- *Eavesdropping area* measures the area where the attacker can achieve PSR higher than a given threshold by eavesdropping on side lobe signals.

3.1 Mesh Network

We begin by showing the effectiveness of eavesdropping in an outdoor mesh network. During transmission, the main lobe points towards RX and side lobes point towards the ground. The eavesdropper moves freely on the ground and

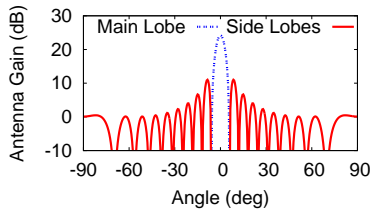


Figure 1: Example of side lobes of a 16×8 array (horizontal plane).

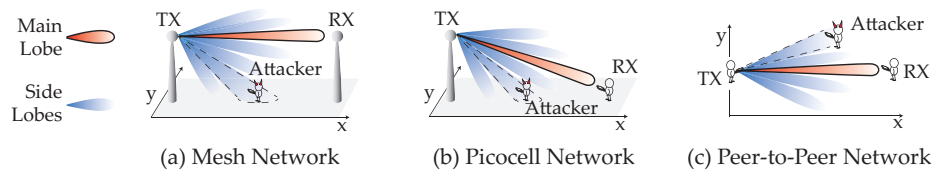


Figure 2: Illustration of three application scenarios we test the eavesdropping attack. Attacker could eavesdrop through side lobes (blue) to decode information transmitted in the main lobe (red).

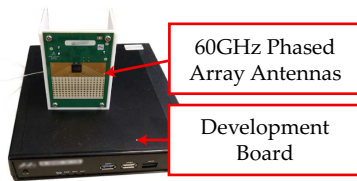


Figure 3: Our 60GHz testbed with 16×8 antenna array.

searches for locations where he could hear side-lobe signals. Fig. 4(a) shows the attacker’s PSR at different locations, and how the eavesdropping area changes.

From the heatmap in the figure, we observe that the attack is proved very effective. In $79m^2$ out of the $200m^2$ examined area, the attacker could successfully decode *at least one* packet. Aggregated, the eavesdropping area accounts for 39.5% of the entire area. Large connected portions allow an attacker to act more stealthily by moving freely through areas as large as $23m^2$ rather than staying in one location.

Note that all eavesdropping areas center along TX’s transmission direction (along the x-axis). This allows the attacker to easily predict vulnerable areas to launch attacks, because side lobes along the x-axis are strong enough for eavesdropping, while other side lobes pointing away from the x-axis suffer higher signal loss ($>13dB$) and become too weak.

We further investigated how the eavesdropping area changes given different PSR thresholds. As shown in the lower figure in Fig. 4(a), the eavesdropping area reduces very slowly as we increase the PSR threshold. When requiring the attacker to achieve $>50\%$ PSR, the eavesdropping area reduces only by 19%, down to $64m^2$. Moreover, in a $55m^2$ area (69.6% of the total eavesdropping area), the attacker could achieve $>95\%$ PSR, the same performance achieved by RX. This further shows the incredible effectiveness of an eavesdropping attack in a mesh network scenario.

Our measurements for the mesh network cover $200m^2$ area and already show the severity of side-lobe eavesdropping. Although not shown in figure, we found that more eavesdropping locations also exist outside the examined area, e.g., $>20m$ away from TX. We leave further investigation of these areas to future work.

3.2 Picocell Network

Fig. 4(b) shows the eavesdropping results in a picocell network scenario. Similar to the mesh network scenario, the attacker could successfully eavesdrop the transmission

in a large area. Within $109m^2$, the attacker could decode at least one packet, which is 54.5% of the entire examined area. An area of $54m^2$ within this $109m^2$ allows the attacker to eavesdrop with $>95\%$ PSR, thus fully recovering the victim’s transmission. The ratio of eavesdropping area to the entire examined area is comparable to the mesh network scenario, which indicates similar levels of effectiveness of the eavesdropping attack.

Interestingly, in both the mesh and picocell networks, the area of connected eavesdropping locations grows larger as the attacker moves away from TX. This seems counter-intuitive, since signals become weaker at farther distances due to propagation loss. However, in outdoor scenarios, the projection of side lobes on the ground grows larger at farther distances. Despite the propagation loss, the side lobes remain strong enough for the attacker to successfully decode the transmission, given the sufficiently high TX power for transmissions at distances over $100m$. This finding appears more obvious in the picocell network because TX’s beams point downwards, causing less propagation loss through side lobes.

Increasing link rate reduces eavesdropping area. Different from the mesh network, where RX remains stationary and achieves at most 1Gbps throughput, the victim RX in picocell is mobile. As RX moves closer to TX, RX could achieve higher SNR and increase data rate up to 1.5Gbps, while maintaining $>95\%$ PSR. We re-configured the testbed to transmit at 1.5Gbps, and measured the corresponding PSR at different locations. The lower figure in Fig. 4(b) shows a smaller eavesdropping area when TX increases data rate from 1Gbps to 1.5Gbps. On average, this reduces the eavesdropping area by $24m^2$. In particular, when requiring the attacker to have $>95\%$, increasing throughput reduces the eavesdropping area from $54m^2$ to $31m^2$. The area reduces because increasing the legit transmission rate also raises the channel quality requirement at the eavesdropper, thus mitigating the attack to some extent. Yet it does not fully solve the problem, as the attacker could still successfully decode packets in a large area.

3.3 Peer-to-Peer Network

Fig. 4(c) shows the eavesdropping performance in a peer-to-peer scenario. In a connected area of $16.6m^2$ the attacker could decode at least one packet. The area is significantly large (83%), compared to the $20m^2$ total examined area. When requiring $>95\%$ PSR, the attacker could still decode the transmission in 65% ($13.1m^2$) of the total area.

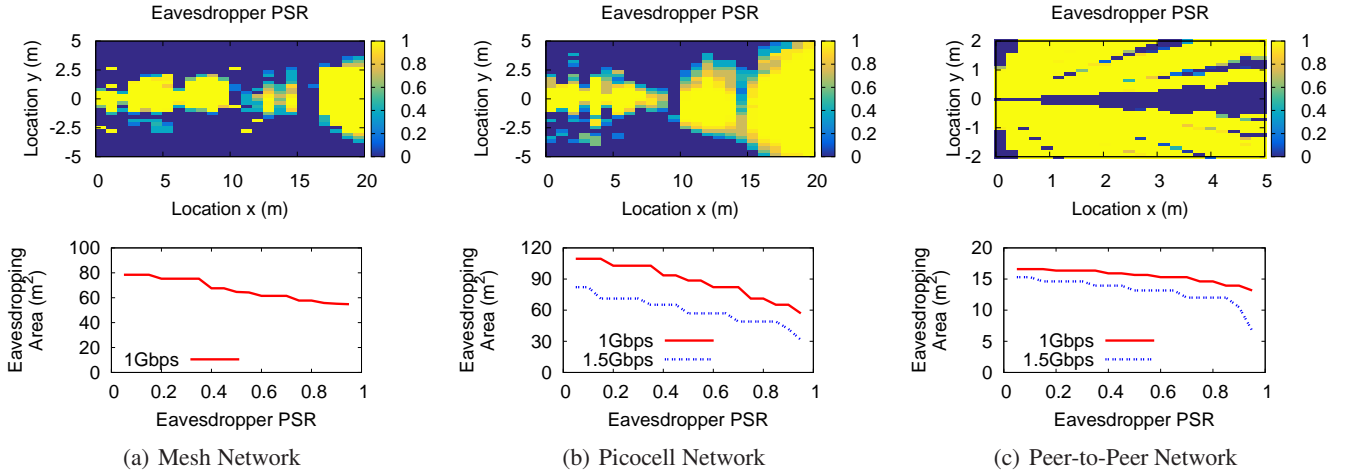


Figure 4: Effectiveness of side-lobe eavesdropping under three mmWave scenarios. For each scenario, the top plot shows attacker’s packet success rate (PSR) at 1Gbps at different side-lobe locations. TX is at (0, 0) and beams towards RX along x-axis. The bottom one shows how the eavesdropping area changes with PSR thresholds at different link rates.

Similar to the picocell scenario, both RX and TX can move freely, causing different distances between RX and TX. This allows higher SNR and higher link rate without degrading RX’s PSR, but again, it cannot remove the eavesdropping area completely. Still, in an area of $7m^2$, the attacker could decode transmissions with $>95\%$ PSR.

Note that the shape of eavesdropping area in the peer-to-peer scenario differs from those in the other two scenarios. This is mainly because TX sits at a much lower height than the other two scenarios. The attacker resides on the same plane of TX and RX, and captures the side-lobe signals on the horizontal plane. As such, the eavesdropping area follows a similar shape of the side-lobe beam pattern (Fig. 1), rather than the circular ones observed in mesh and picocell networks. This observation of different shapes within eavesdropping areas could better guide the attacker’s predictions for where to launch attacks based on a targeted scenario.

Although the eavesdropping area in an indoor scenario accounts for a larger portion of the examined area than the outdoor scenarios, its absolute size is significantly smaller, thus with less potential threat. Moreover, 60GHz signals can hardly penetrate walls, so the eavesdropping area for the indoor scenario remains bounded by its room size, further restricting the attacker’s mobility and effectiveness of eavesdropping. Therefore, side-lobe eavesdropping proves much more severe in the prior two outdoor scenarios.

3.4 Summary

In all scenarios, we find that a passive attacker could effectively eavesdrop transmissions with very high PSR in a large area. This shows that despite the directional nature of mmWave beamforming transmission, side lobes still expose a significant amount of information. Increasing transmission rate slightly mitigates the threat, but cannot effectively defend against the eavesdropping attack.

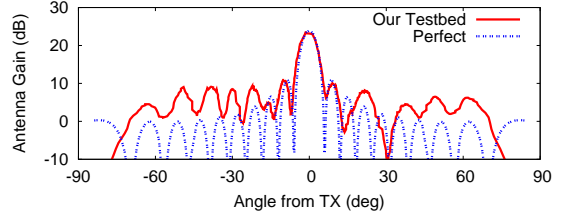


Figure 5: Antenna artifacts cause side lobe distortions.

4. IMPACT OF RADIO HARDWARE

So far we have empirically measured the eavesdropping area using off-the-shelf 60GHz devices (16×8 phased arrays). In this section, we further explore whether upgrading array hardware can help reduce the impact of eavesdropping attacks. Specifically, there are two immediate ways to improve mmWave array hardware and reduce side-lobe emissions: (1) removing implementation artifacts from the antenna radiation pattern, (2) increasing the number of antenna elements. Fig. 5 compares the ideal antenna radiation pattern and that of our current hardware. While the current hardware faces distortions on side-lobe emissions, the ideal array implementation would produce weaker, less detectable side lobes. Similarly, increasing the number of antennas can also reduce the emission power of side lobes [16], thereby reducing the performance of an eavesdropping attack.

In the following, we study how upgrading radio hardware would reduce the eavesdropping effectiveness. To emulate hardware configurations different from our testbed, we used trace-driven simulations. Specifically, we apply the Friis free-space propagation model [22] to compute an attacker’s SNR at different locations. All of our testbed measurements, along with prior works [42, 40], show that this model can accurately estimate the SNR in line-of-sight with very small errors ($\pm 1dB$). At each location, we map simulated SNR to PSR using the empirical correlation derived from previ-

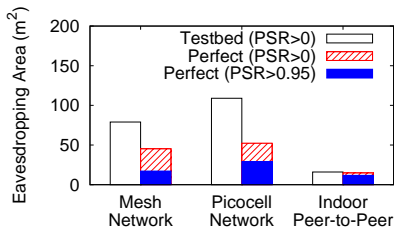


Figure 6: Perfect antennas help mitigate eavesdropping but not avoid it.

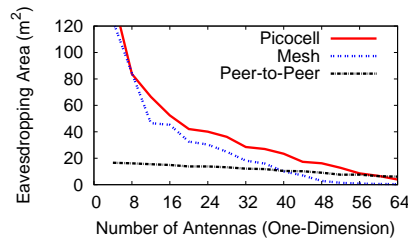


Figure 7: Increasing number of antennas helps reduce eavesdropping area.

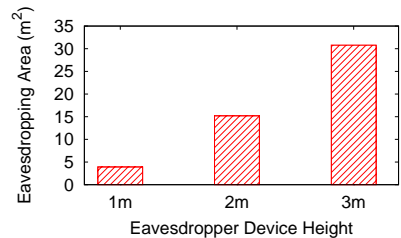


Figure 8: Attacker can raise device high to enlarge eavesdropping area.

ous testbed experiments. We verified that this correlation remains stable and accurate across different application scenarios and link rates. Our simulations follow the same configuration in §2, with altered hardware aspects. We also expanded the experiments by varying the height of the eavesdropping device and RX’s locations.

4.1 Perfect Antennas without Artifacts

First we simulated eavesdropping attacks on three application scenarios, using perfect antennas without artifacts. Fig. 6 shows the eavesdropping areas for different scenarios, compared with our testbed measurements. We only present results with 1Gbps, and omit those from other data rates as they show similar findings.

Comparing eavesdropping areas using perfect antennas and our testbed, we found eliminating hardware artifacts reduces the eavesdropping area. In the mesh and picocell network scenarios, the eavesdropping area reduced by 43% and 52% respectively. However, the area for the indoor peer-to-peer scenario reduced by only 4%, as for short-range indoor communications, TX’s power (with $23dBm$ EIRP) at side lobes is high enough to allow eavesdropping.

Despite the reduced eavesdropping area, we find the remaining area is still large enough for attackers to move around while achieving high PSR. In mesh, picocell, and peer-to-peer scenarios, an attacker could achieve full recovery of the transmission ($>95\%$ PSR) in $45m^2$, $52m^2$, and $15m^2$ respectively. Thus, *removing hardware artifacts cannot fully defend against eavesdropping*.

4.2 Increasing Number of Antenna Elements

In addition to removing artifacts from hardware, we increased the number of antennas, and tested if the combination of these two techniques could defend against the eavesdropping attacks. Fig. 7 shows how the eavesdropping area (with $PSR > 0$) changes as we increase the number of antennas in the horizontal plane (our testbed uses 16 antennas in this plane). We find that in all our application scenarios, eavesdropping area decreases monotonically as we add more antennas. For example, in the picocell network scenario, using 64 antennas (compared to 16 in our testbed) effectively reduces the eavesdropping area from $52.39m^2$ down to $3.91m^2$. This confirms the theory that more antenna elements reduce side lobes’ beam width and emission power, resulting in shrinking the area where an attacker could re-

ceive the side-lobe signals.

As well as incurring larger hardware implementation cost and size, *increasing the number of antennas does not fully prevent an eavesdropping attack*. For instance, in both mesh and picocell scenarios, a simple yet effective method for attacker is to raise the eavesdropping device to get closer to TX and receive stronger signals. This results in higher SNR than eavesdropping on the ground, and the attacker could achieve better eavesdropping results. Fig. 8 shows its effect in the picocell scenario. Even though TX uses 64 perfect antennas (in the horizontal plane), an attacker could increase the eavesdropping area from $3.91m^2$ to $15.2m^2$ by moving the device from in-hand position (1m) to above-head (2m). If attacker uses drones to further raise the device height, the eavesdropping area increases to $30.8m^2$. We observed similar improvement in mesh networks. As such, even after reconfiguring hardware with significant cost, an attacker could still successfully eavesdrop in large area. This poses a serious security threat as simple methods, like holding the device higher, allow attackers to advance beyond hardware upgrades. So we need new defense mechanisms.

5. ANALYSIS OF EXISTING DEFENSES

Existing defenses focus on adding *artificial noises* to side-lobe signals to prevent attackers from decoding useful information [13, 21, 24, 31, 37, 39, 41]. They fall under two categories, depending on how the noise is generated: (1) antenna-based defenses and (2) RF-chain-based defenses⁵. In this section, we analyze these defenses to study whether they are practical and effective defending against side-lobe eavesdropping. We summarize them in Table 2.

Antenna-Based Defenses. This defense creates noisy side lobes by changing the radiated signals from a subset of antenna elements. During transmission, TX either disables [13, 37] or flips the phase [21] of a random subset of antennas. This produces randomized radiation patterns on side lobes, with minimal impact on normal transmissions⁶.

Antenna-based defenses require TX to change the selected antenna subset very frequently, often on a per-symbol ba-

⁵ An RF (radio-frequency) chain refers to a set of physical hardware components for wireless signal processing, bridging between the antenna array and radio baseband.

⁶ Due to space limit, we omit details about this defense. We refer interested readers to related work for more information.

sis, *i.e.* at the time scale of *sub-nanoseconds*. Less frequent switching keeps signals within a packet highly correlated with each other. This could allow the attacker to simply estimate the wireless channel, or guess the correlation constant to recover the transmission. Despite the effectiveness, switching at a per-symbol frequency incurs extremely high cost in hardware and power. Today’s hardware can only support packet-level switching (10s of nanoseconds) for the same reason, making antenna-based defenses impractical.

Despite the impracticality, we implemented the defenses in simulation. We found it effectively defends against single-device side-lobe eavesdroppers, regardless of where the attack is launched. However, it remains vulnerable to advanced attacks. For instance, attack can use multiple *synchronized* devices to measure side-lobe signals at different angles, undo the effects of antenna randomization on a per-symbol basis, and recover the packets. The key is to decode the antenna selections for transmission from measurements, as there is a limited number of antenna subset selections.

RF-Chain-Based Defenses. Unlike antenna-based defenses, these defenses add *additional* RF chains to generate noise and do not need randomizations in TX’s radiation pattern. They “jam” the eavesdropper at TX’s side lobes, so the attacker can only receive a mixture of transmitted signals and noise signals. For mmWave hardware, this adds significant complexity and cost in RF signal processing components, increasing the hardware cost and power requirements. Despite that previous work [14, 21] reduces the hardware requirement, these defenses [21, 24, 39, 41] remain costly and power-demanding.

We found in simulations that RF-chain-based defenses effectively defend against single-device eavesdroppers. Although, TX’s side lobes have gaps in between, which nulls the transmitted signals. An advanced attacker can exploit this and search for only noise signals. He could then perform noise cancellation with only two synchronized receivers: one listening to only noise and the other eavesdropping the mixed noise and legit signals. The attack becomes more difficult when TX uses over two RF chains to generate noise. Noise from different RF chains would mix together and becomes difficult to isolate. Still, this countermeasure comes at an even higher cost in mmWave hardware and device power.

Category	Defense Requirement		Vulnerability	
	# of RF Chains	Antenna Switching Frequency	# of Sync. Devices to Attack	Info. Required for Attack
No Defense	1	-	1	side-lobe signals
Antenna-Based	1	per-symbol	N	signals at N locations
RF-Chain-Based	>2	-	2	noise signals at N locations

Table 2: Summary and vulnerabilities of different defense mechanisms. N is the number of TX antennas.

6. RELATED WORK

Security Analysis in mmWave Eavesdropping. Existing works to study mmWave eavesdropping either perform simulations [13, 18, 19, 21, 24, 25, 37, 38, 41] or use horn antennas [35], which have no side lobes. Differing from these, we are the first to study mmWave side-lobe eavesdropping from actual measurements, using commercial 60GHz phased arrays in real-world application scenarios.

Many of these proposed defenses against mmWave eavesdropping, *i.e.* using antenna-based [13, 21, 37] or RF-chain-based designs [21, 24, 38, 41] assume a naive single-device attacker. Our work analyzes these proposals and finds these methods either as vulnerable to advanced attackers with multiple synchronized devices, or they introduce significant hardware overhead and cost. Thus, these defenses are not applicable to mmWave transmissions.

Eavesdropping in Low-Frequency RF Bands. Eavesdropping is more prevalent and easier in lower frequency bands, *e.g.*, Wi-Fi and cellular, due to its omni-directional signals. Many previous works propose defense mechanisms using jamming, which injects artificial noise towards the attackers [20, 27, 39]. Although different techniques are used, *e.g.*, a separated jammer synchronized with the transmitter [23], cooperative devices or relays [20, 27], these defensive mechanisms all require a high number of RF chains. Despite the acceptably minimized hardware cost in commodity Wi-Fi and cellular devices, the cost of these defenses remains extremely high in the context of mmWave.

7. CONCLUSION AND FUTURE WORK

Despite an initial step to investigate mmWave side-lobe eavesdropping with real measurements, we already find it proves to be a much greater threat than we expected. We hope our results draw the attention of the community and shed light on the future development of mmWave communications. Moving forward, many open challenges remain.

Potential Defenses. Despite existing proposals, we lack a practical and secure solution against side-lobe eavesdropping. Other than reducing the RF chain cost in mmWave communications, a possible alternative could leverage the antenna artifacts. Designing specific artifacts in hardware could resist the attack since we saw earlier that artifacts may alter the shape of side lobes. The artifacts should be carefully designed so the normal transmission remains unaffected.

Empirical Validation of Advanced Attacks. We briefly described and simulated two types of advanced attacks, *i.e.* antenna randomization attack and noise cancellation attack. While other advanced attacks remain possible, current mmWave hardware is not flexible enough to implement these attacks. Also, our device does not report bit error rate (BER) which may shed light on more fine-grained insights as [26] did. We hope more flexible hardware becomes available soon, so we can empirically validate the attacks with consideration of antenna artifacts, which may affect the attacks’ performance.

8. REFERENCES

- [1] 60ghz wireless technology overview. <http://www.mmwaves.com/products.cfm/product/20-194-0.htm>.
- [2] Aircrack. <https://www.aircrack-ng.org/>.
- [3] Dell wireless dock wigi. <http://i.dell.com/sites/doccontent/consumer/merchandizing/en/Documents/Dell-Wireless-Dock-WiGig-spec-sheet.pdf>.
- [4] Facebook's terragraph. <https://techcrunch.com/2016/04/13/terragraph/>.
- [5] Google fiber considers gigabit wifi to cheaply cover last mile. <https://www.engadget.com/2016/06/09/google-fiber-considers-gigabit-wifi-to-cheaply-cover-last-mile/>.
- [6] IEEE 802.11 Task Group AD. http://www.ieee802.org/11/Reports/tgad_update.htm.
- [7] San jos partners with facebook for high-speed outdoor wi-fi. <https://gcn.com/articles/2016/04/18/san-jose-facebook.aspx>.
- [8] Talon ad7200 multi-band wi-fi router. http://www.tp-link.com/us/products/details/cat-5506_AD7200.html.
- [9] Wilocity: 60ghz wireless revolution begins at ces. http://news.cnet.com/8301-30685_3-57326718-264/wilocity-60ghz-wireless-revolution-begins-at-ces/.
- [10] Wireless htc vive tested: One of vr's problems solved, but two remain. <https://arstechnica.com/gadgets/2017/02/htc-vive-wireless-tested-review/>.
- [11] Your wi-fi's wpa2 encryption can be cracked offline: Here's how. <https://www.howtogeek.com/202441/your-wi-fi%E2%80%99s-wpa2-encryption-can-be-cracked-offline-here%E2%80%99s-how/>.
- [12] ABARI, O., BHARADIA, D., DUFFIELD, A., AND KATABI, D. Enabling high-quality untethered virtual reality. In *Proc. of NSDI* (2017).
- [13] ALOTAIBI, N. N., AND HAMDY, K. A. Switched phased-array transmission architecture for secure millimeter-wave wireless communication. *IEEE Transactions on Communications* 64, 3 (2016).
- [14] AYACH, O. E., RAJAGOPAL, S., ABU-SURRA, S., PI, Z., AND HEATH, R. W. Spatially sparse precoding in millimeter wave mimo systems. *IEEE Transactions on Wireless Communications* 13, 3 (2014).
- [15] BAIRD, C., AND RASSWEILER, G. Adaptive sidelobe nulling using digitally controlled phase-shifters. *IEEE Transactions on Antennas and Propagation* 24, 5 (1976).
- [16] BALANIS, C. A. *Antenna theory: analysis and design*. John Wiley & Sons, 2016.
- [17] BISSIAS, G., LIBERATORE, M., JENSEN, D., AND LEVINE, B. N. Privacy vulnerabilities in encrypted http streams. In *Proc. of PET* (2005).
- [18] DAI, H.-N., LI, D., AND WONG, R. C.-W. Exploring security improvement of wireless networks with directional antennas. In *Proc. of LCN* (2011).
- [19] DAI, H.-N., WANG, Q., LI, D., AND WONG, R. C.-W. On eavesdropping attacks in wireless sensor networks with directional antennas. *International Journal of Distributed Sensor Networks* 9, 8 (2013).
- [20] DONG, L., HAN, Z., PETROPULU, A. P., AND POOR, H. V. Cooperative jamming for wireless physical layer security. In *Proc. of SSP* (2009).
- [21] ELTAYEB, M. E., CHOI, J., AL-NAFFOURI, T. Y., AND HEATH, R. W. Enhancing secrecy with multi-antenna transmission in millimeter wave vehicular communication systems. *IEEE Transactions on Vehicular Technology* PP, 99 (2017).
- [22] FRIS, H. T. A note on a simple transmission formula. In *Proc. of IRE* 34, 5 (1946), 254-256.
- [23] GOLLAKOTA, S., AND KATABI, D. *ijam: Jamming oneself for secure wireless communication*. Tech. rep., Computer Science and Artificial Intelligence Laboratory Technical Report, 2010.
- [24] JU, Y., WANG, H. M., ZHENG, T. X., AND YIN, Q. Secure transmissions in millimeter wave systems. *IEEE Transactions on Communications* 65, 5 (2017).
- [25] KIM, M., HWANG, E., AND KIM, J.-N. Analysis of eavesdropping attack in mmwave-based wpans with directional antennas. *Wireless Networks* 23, 2 (2017).
- [26] LACURTS, K., AND BALAKRISHNAN, H. Measurement and analysis of real-world 802.11 mesh networks. In *Proc. of IMC* (2010).
- [27] LAI, L., AND EL GAMAL, H. The relay-eavesdropper channel: Cooperation for secrecy. *IEEE Trans. Inf. Theor.* 54, 9 (2008).
- [28] LIBERATORE, M., AND LEVINE, B. N. Inferring the source of encrypted http connections. In *Proc. of CCS* (2006).
- [29] MARZI, Z., MADHOW, U., AND ZHENG, H. Interference analysis for mm-wave picocells. In *Proc. of GLOBECOM* (2015).
- [30] NAKHILA, O., ATTIAH, A., JINZ, Y., AND ZOUX, C. Parallel active dictionary attack on wpa2-psk wi-fi networks. In *Proc. of MILCOM* (2015).
- [31] RAMADAN, Y. R., IBRAHIM, A. S., AND KHAIRY, M. M. Rf beamforming for secrecy millimeter wave miso-ofdm systems. In *Proc. of ICC* (2016).
- [32] RASEKH, M. E., MARZI, Z., ZHU, Y., MADHOW, U., AND ZHENG, H. Noncoherent mmwave path tracking. In *Proc. of HotMobile* (2017).
- [33] SHAKED, Y., AND WOOL, A. Cracking the bluetooth pin. In *Proc. of MobiSys* (2005).
- [34] SHELDON, F. T., WEBER, J. M., YOO, S.-M., AND PAN, W. D. The insecurity of wireless networks. *IEEE Security & Privacy* 10, 4 (2012).
- [35] STEINMETZER, D., CHEN, J., CLASSEN, J., KNIGHTLY, E., AND HOLLICK, M. Eavesdropping with periscopes: experimental security analysis of highly directional millimeter waves. In *Proc. of CNS* (2015).
- [36] TEWS, E., AND BECK, M. Practical attacks against wpa and wpa. In *Proc. of WiSec* (2009).
- [37] VALLIAPPAN, N., LOZANO, A., AND HEATH, R. W. Antenna subset modulation for secure millimeter-wave wireless communication. *IEEE Transactions on Communications* 61, 8 (2013).
- [38] WANG, C., AND WANG, H. M. Physical layer security in millimeter wave cellular networks. *IEEE Transactions on Wireless Communications* 15, 8 (2016).
- [39] ZHANG, X., ZHOU, X., AND MCKAY, M. R. Enhancing secrecy with multi-antenna transmission in wireless ad hoc networks. *IEEE Transactions on Information Forensics and Security* 8, 11 (2013).
- [40] ZHOU, X., ZHANG, Z., ZHU, Y., LI, Y., KUMAR, S., VAHDAT, A., ZHAO, B. Y., AND ZHENG, H. Mirror mirror on the ceiling: Flexible wireless links for data centers. In *Proc. of SIGCOMM* (2012).
- [41] ZHU, Y., WANG, L., WONG, K., AND HEATH, R. W. Secure communications in millimeter wave ad hoc networks. *IEEE Transactions on Wireless Communications* 16, 5 (2017).
- [42] ZHU, Y., ZHANG, Z., MARZI, Z., NELSON, C., MADHOW, U., ZHAO, B. Y., AND ZHENG, H. Demystifying 60GHz outdoor picocells. In *Proc. of MobiCom* (2014).